Japanese Journal of Applied Physics

The Japan Society of Applied Physics

REGULAR PAPER

Efficient ab initio plus analytic calculation of the effect of GaN layer tensile strain in AlGaN/GaN heterostructures

Japanese Journal of Applied Physics **58**, 094001 (2019) **REGULAR PAPER**
https://doi.org/**10.7567/1347-4065/ab39d0**

Efficient ab initio plus analytic calculation of the effect of GaN layer tensile strain in AlGaN/GaN heterostructures

Mihir Date[1], Sudipta Mukherjee[2], Joydeep Ghosh[2], Dipankar Saha[2], Swaroop Ganguly[2*], Apurba Laha[2], and Prasenjit Ghosh[3]

[1]*Department of Chemical Engineering, Indian Institute of Science, Mathikere, Bangalore, 560012, India*
[2]*Department of Electrical Engineering, Indian Institute of Technology Bombay, 400076 Mumbai, India*
[3]*Department of Physics, Indian Institute of Science Education and Research Pune, Pune, 411008 India*

[*]E-mail: swaroop.ganguly@gmail.com

Received July 11, 2019; revised August 5, 2019; accepted August 8, 2019; published online August 27, 2019

We have addressed the existing ambiguity regarding the effect of tensile strain in the underlying GaN layer on $Al_xGa_{1-x}N$/GaN heterostructure properties. The bandgaps and band-offsets for $Al_xGa_{1-x}N$ on strained GaN were first computed using density functional theory (DFT), in the generalized gradient approximations (GGA) and hybrid functional Gaussian–Perdew–Burke–Ernzerhof (Gau–PBE) regimes. We propose a simple model to relate the GGA and Gau–PBE bandgaps, which is used to determine the realistic bandgaps of strained AlGaN. The bandgaps and band-offsets from the DFT calculations are then used to analytically calculate the two-dimensional electron gas density in an $Al_xGa_{1-x}N$/GaN hetero-interface. Our bandstructure calculations show that it is not possible to induce significant change in band-offsets through strain in the GaN layer. The charge-density calculations indicate that such strain can, however, modulate the polarization charge and thereby enhance the 2DEG density at the AlGaN/GaN interface substantially. © 2019 The Japan Society of Applied Physics

Supplementary material for this article is available online

1. Introduction

In the past few decades, GaN-based heterostructure device technologies have been developed intensively for high-frequency, high-voltage, and opto-electronic device applications. Alloying this semiconductor with AlN produces $Al_xGa_{1-x}N$ where x is the Aluminium mole fraction, and the heterostructure which can be formed between AlGaN and GaN is the key in realizing high electron mobility transistors (HEMTs). In these devices, a two-dimensional electron gas (2DEG) is formed at the hetero-interface due to large polarization fields coupled with the donor-like surface states.[1,2] The growth of these AlGaN/GaN heterostructures on Si substrates has been a coveted goal from the points of view of cost and heterogeneous integration.[3] Now, it is usual to localize strain, and related defects, away from the AlGaN/GaN hetero-interface when growing on a lattice mismatched substrate like Si or sapphire, by grading the GaN layer; this layer is therefore conventionally assumed to provide a relaxed virtual substrate. However, even if a thick/graded GaN layer perfectly neutralizes the mismatch-induced strain, it may not be free from any process-induced strain. It has been shown experimentally that thinning of the underlying Si substrate—which would be desirable for many heterogeneously integrated applications—can lead to a tensile strain in the GaN layer, with consequent increase in 2DEG concentration and mobility.[4] Lee et al.[5] have also reported that, in AlGaN/AlN/GaN heterostructures, the strain in the GaN layer significantly affects the 2DEG concentration and electron mobility. Recent studies carried out by Kadir et al.[6] have concluded that it may be therefore more accurate to assume the Si substrate as the reference material than GaN in order to account for the stresses at the GaN-Si interface. Liu et al.,[7] on the other hand, has suggested that referencing Si does not offer any significant advantage. We seek to provide a theoretical basis to unambiguously comprehend the experimental data and to derive predictive insights for heterostructure device design.

Physics-based models have been developed and extensive simulations are performed by several groups to predict the 2DEG density as well as the bare surface barrier height in different GaN-based heterostructures.[8–12] Indeed, the 2DEG density depends on the bandgap, lattice mismatch, and the AlGaN surface state parameters. Now, as mentioned above, the GaN substrate has usually been considered relaxed. However, in view of the aforementioned experimental reports, it becomes imperative to investigate and clarify how strain in the GaN layer—due to process-related reasons if the lattice mismatch can be assumed to be neutralized—impacts the 2DEG concentration in the AlGaN/GaN heterostructure. It is practical to imagine that the GaN layer could be strained due to a combination of various factors: imperfect localization of lattice mismatch-induced stress, defects in the heterostructure, and other residual stresses arising from the growth and processing steps. Further, our results confirm benefits to straining the GaN layer—so it could conceivably be incorporated by heterostructure design in the future. Therefore, strain in the GaN is an input parameter in our calculations, representing the cumulative effect of the above possibilities. We calculate the impact of strain and Al mole fraction on the band offsets and thereby calculate the 2DEG density. The very next Sect. lays out the bandstructure calculation methodology and the resulting bandgap and band offsets. The following one deals with charge-density calculations that take these as inputs to obtain the polarization charge and 2DEG density.

2. Electronic structure of $Al_xGa_{1-x}N$

2.1. Computational methodology

Our bandstructure calculations were performed using plane-wave based density functional theory, as implemented in the software package QUANTUM ESPRESSO.[13,14] We have employed a norm-conserving electron-ion interaction pseudopotential within the generalized gradient approximation (GGA) exchange-correlation functional, described by the Perdew–Burke–Erzenhoff (PBE)[15] parametrization of the

GGA functional. While this yields the correct trends in the bandgaps as shown in Fig. 1, the GGA approximation, as is evident from Fig. 1, underestimates bandgaps severely. This issue is resolved by using a hybrid functional Gaussian–Perdew–Burke–Ernzerhof (Gau–PBE). We performed the calculations for the unstrained AlGaN using the relaxed lattice parameters, whereas to simulate AlGaN on top of GaN, we performed calculations within the pseudomorphic approximation and therefore the in-plane lattice parameter (say, a) of AlGaN was forced to be same as that of GaN. For computing the electronic structure of strained GaN, AlGaN and AlN, we consider the tensile strain as a percentage increment in the in-plane lattice constant a, while using the optimised (relaxed) out-of-plane lattice constant c. The cut-offs for wavefunction and charge-density were 75 Ry and 300 Ry respectively, for all our simulations. For calculating the bandstructure of GaN, we used the $12 \times 12 \times 8$ Monkhorst–Pack (MP)[16] **k**-mesh. We consider three mole fractions of Al- 0.25, 0.5 and 0.75 in this work and to calculate the bandstructure of these, we used a $2 \times 2 \times 1$ supercell. For the supercell, we used a $6 \times 6 \times 8$ MP. For calculations involving the hybrid functional, we construct a **q**-mesh (in the reciprocal space) of $3 \times 3 \times 2$ for GaN and $2 \times 2 \times 2$ for AlGaN respectively, for each **k**-point in the Brillouin Zone, for the integration of the Fock operator.

2.2. Structure of GaN, AlGaN and AlN

The lattice parameters of our relaxed structures for the Wurtzite GaN are $a = 3.21$ Å and $c = 5.231$ Å respectively, and that for AlN are $a = 3.126$ Å and $c = 5.011$ Å respectively, which are an excellent match with reported experimental and theoretical values.[1,5,17,21–23]

To demonstrate the cases of $Al_{0.25}Ga_{0.75}N$, $Al_{0.5}Ga_{0.5}N$, and $Al_{0.75}Ga_{0.75}N$ two, four and six Ga atoms are substituted by Al atoms in the supercell, respectively. We identify that there are 3(28), 6(70) and 3(28) symmetry inequivalent configurations (total number of configurations) of the Al mole fraction values of 0.25, 0.5 and 0.75 respectively. Lattice parameters and atomic positions of these structures are relaxed (see supplemental information, available online at stacks.iop.org/JJAP/58/094001/mmedia) and the most energetically stable structure is chosen as shown in Fig. 2.

The in-plane lattice constant (a) agrees well with the experiments and also with Vegard's law (shown by the discontinuous line in Fig. 3). The out of plane lattice constant (c) appears to deviate from the experimental reports, and is fit to a quadratic expression [the discontinuous line in Fig. 3(b)]: $c/a(x) = 1.603x + 1.626(1-x) + bx(1-x)$, where b is the strength of deviation away from linear trends. The maximum error obtained for such a fit is less than 0.48%, for 0.5 mole fraction of Al. For all Al mole fractions, substitution of Ga by Al does not influence the Ga–N structure, however, the Al–N bond gets stretched by about 3%, as compared to that in AlN. The average bond length in AlGaN, from our calculations is good match with the linear mixing scheme:[24]

$$d_{\mathrm{AlGaN}} = d_{\mathrm{AlN}}x + d_{\mathrm{GaN}}(1 - x). \tag{1}$$

The general observations for all mole fractions of Al, upon straining AlGaN, suggest that the Al–N bond length reduces, while the Ga–N bond length increases.

In case of strained $Al_{0.25}Ga_{0.75}N$, for strain $\varepsilon_{\mathrm{GaN}}$ of 1%, both the Al and N atoms move close to each other, while the Ga atom moves out of the plane stretching the Ga–N bond. This causes the Al–N bond length to reduce by ≈2% and the Ga–N bond increases by ≈1.7%.

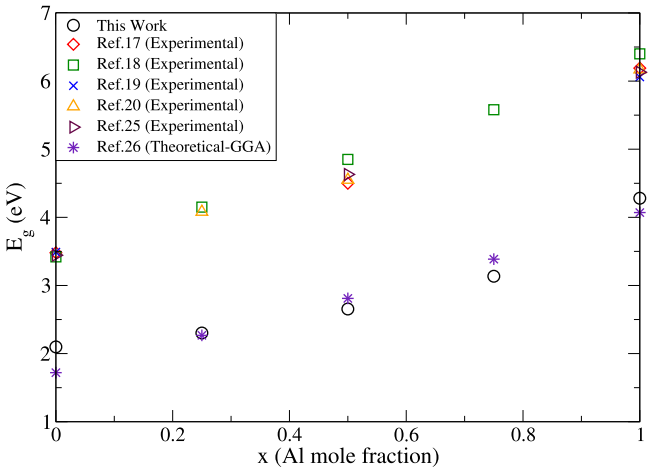

Fig. 1. (Color online) A comparison between GGA bandgaps of free-standing $Al_xGa_{1-x}N$ (obtained from this work) and those obtained from experiments in Ref. 17–20,25, and GGA bandgaps, as reported in Ref. 26. It is clear that though GGA functional underestimates the band gap, it correctly represents the trends.

2.3. Bandstructure calculations

Our bandgaps calculated for AlN, GaN, and $Al_{0.25}Ga_{0.75}N$ using Gau–PBE agree well with the experimental observations (ref: Table I). However, computing bandgaps for compositions and strains with hybrid functionals are computationally expensive. In order to circumvent this, we present a general model for AlGaN which successfully predicts realistic bandgaps without requiring these heavy computations to be performed.

Our GGA band gaps reveal that the ratio $\Phi(\varepsilon) = E_g^{\mathrm{GGA}}(x, \varepsilon)/E_g^{\mathrm{GGA}}(x, 0)$ including the effect of strain could be estimated to be a linear function, independent of Al mole fraction as shown in Fig. 4, and is described by

$$\Phi(\varepsilon_{\mathrm{GaN}}) = 1 - 0.049\varepsilon_{\mathrm{GaN}}. \tag{2}$$

The maximum error obtained from the above fit is approximately 0.2%. This allows us to write the GGA bandgap as a separable function of two independent variables, namely the Al mole fraction (x) and the strain in GaN (ε). Thus, we have:

$$E_g^{\mathrm{GGA}}(x, \varepsilon) = E_g^{\mathrm{GGA}}(x, 0) \cdot \Phi(\varepsilon). \tag{3}$$

Further, comparing the PBE and Gau–PBE band gaps as a function of the tensile strain (Fig. 5) for a given Al mole fraction ($x = 0.25$ for this case) we find that the variation in the bandgap with tensile strain in GaN ($\varepsilon_{\mathrm{GaN}}$) has the same weakly linear trend irrespective of which exchange-correlation functional is used. The slopes of the linear fit obtained for the PBE and Gau–PBE are 0.122 and 0.114 respectively, where the misfit lies in tolerable experimental error regime. This motivates us to write:

$$E_g^{\mathrm{X}}(x, \varepsilon) = E_g^{\mathrm{X}}(x, 0) - \Delta(x)\varepsilon, \tag{4}$$

where, $E_g^{\mathrm{X}}(x, \varepsilon)$ is the bandgap, dependent on strain and Al mole fraction x and $\Delta(x)$ is the composition dependent slope of the linear fits in Fig. 5. The index "X" denotes the choice of exchange-correlation function used—GGA or hybrid functional.

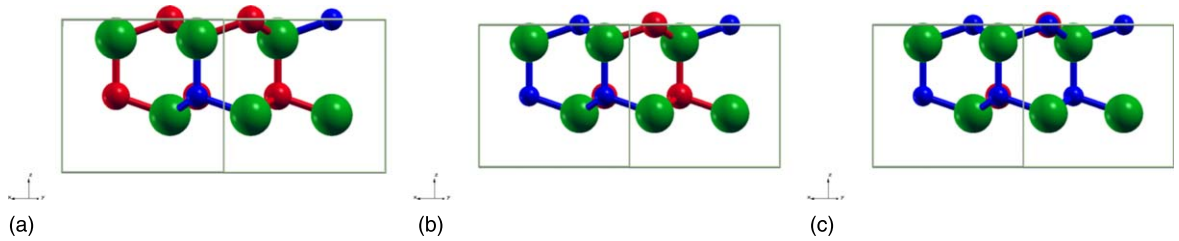

Fig. 2. (Color online) Lowest energy configurations for AlGaN having Al mole fractions of 0.25 (a), 0.5 (b) and 0.75 (c). The Al, Ga and N atoms are denoted by blue, red and green spheres respectively.

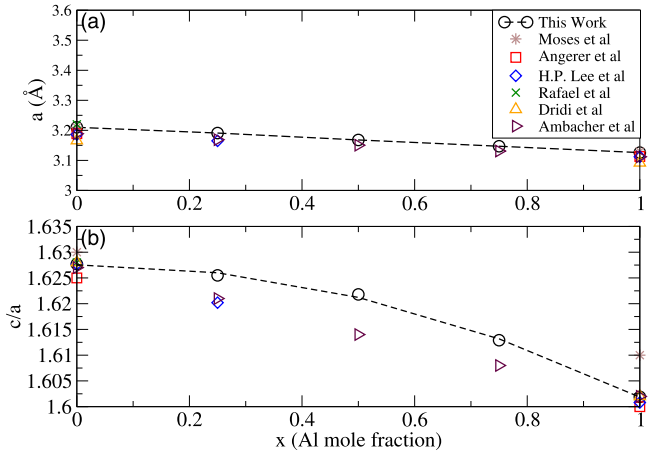

Fig. 3. (Color online) Variation in lattice parameters of AlGaN with Al mole fraction.

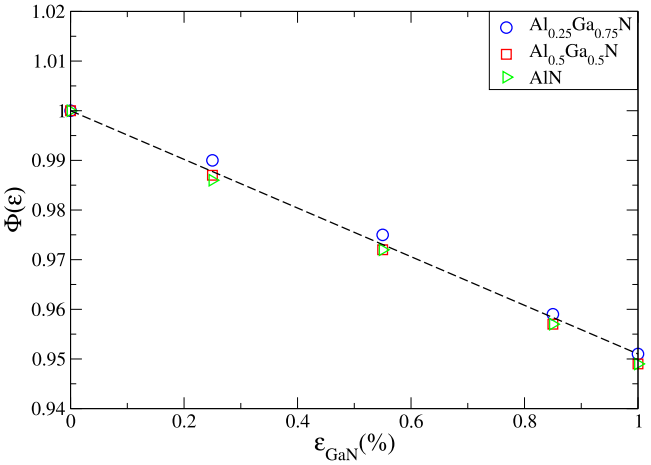

Fig. 4. (Color online) Ratio of the strained to the relaxed GGA bandgap $\Phi(\varepsilon) = E_g^{\mathrm{GGA}}(x, \varepsilon)/E_g^{\mathrm{GGA}}(x, 0)$, as a function of ε; indicating no dependence on the Al mole fraction x.

Then, substituting "GGA" for "X" in Eq. (4), and using Eq. (3), we have:

$$E_g^{\mathrm{GGA}}(x, 0) - \Delta(x)\varepsilon = E_g^{\mathrm{GGA}}(x, 0) \cdot \Phi(\varepsilon). \tag{5}$$

This may be rewritten as follows:

$$\Delta(x) \cdot \varepsilon = E_g^{\mathrm{GGA}}(x, 0)[(1 - \Phi(\varepsilon))]. \tag{6}$$

Now, substituting "Hybrid" for "X" in Eq. (4), and using Eq. (6) therein, one can obtain E_g^{Hybrid} as follows:

$$E_g^{\mathrm{Hybrid}}(x, \varepsilon) = E_g^{\mathrm{Hybrid}}(x, 0) - [E_g^{\mathrm{GGA}}(x, 0)(1 - \Phi(\varepsilon))]. \tag{7}$$

Lastly, from the inset of Fig. 5, we see that the difference between the Hybrid Functional and GGA bandgaps of relaxed AlGaN varies almost linearly with the Al mole fraction x. We may write this as:

$$E_g^{\mathrm{Hybrid}}(x, 0) = E_g^{\mathrm{GGA}}(x, 0) + A + Bx, \tag{8}$$

where A and B are constants, which may be read-off from Fig. 1. Substituting Eq. (8) into Eq. (7) and simplifying, we get:

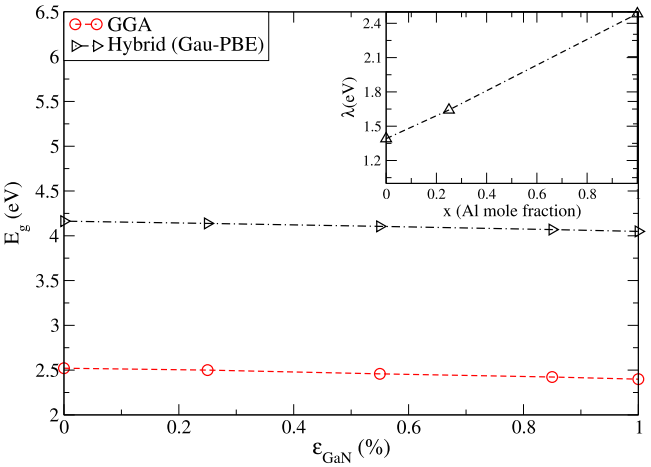

Fig. 5. (Color online) Variation in band gap as a function of tensile strain for AlGaN with with 25% Al with PBE and Gau–PBE. The plot indicates that the two bandgaps are separated by a constant value across the range of tensile strain. The inset figure shows that this separation ($\lambda = E_g^{\mathrm{Hybrid}} - E_g^{\mathrm{GGA}}$) is purely dependent (linearly) on Al mole fraction.

$$E_g^{\mathrm{Hybrid}}(x, \varepsilon) = A + Bx + E_g^{\mathrm{GGA}}(x, 0) \cdot \Phi(\varepsilon), \tag{9}$$

Table I. Bandgaps obtained for GaN, $Al_{0.25}Ga_{0.75}N$ and AlN by employing the hybrid functional Gau–PBE method. x denotes the Al mole fraction.

x	Gau–PBE E_g(eV)(GGA E_g) This work	Reported bandgaps(eV) (Hybrid Functional)	Reported bandgaps(eV) (Experimental)
0	3.49	3.24,[21] 3.23[23]	3.48,[19] 3.49,[20] 3.44[17]
0.25	4.08	—	4.08[27]
1	6.25	5.61[23]	6.19,[19] 6.06,[20] 6.17[27]

where $\Phi(\varepsilon)$ may be read-off from Fig. 4. We validate the reproducibility of the strain function $\Phi(\varepsilon)$ by comparing its values extracted from Fig. 4 and Eq. (7). Such a comparison over the entire composition range gives a maximum error of $\approx$0.4%.

We further study the dependence of the conduction band (CB) -offset on the tensile strain in GaN. The CB offset is defined as the difference in CB edges of AlGaN and GaN, measured with reference to the Fermi level. The Fermi level both the cases is defined as $E_F = \frac{E_C + E_V}{2}$. Upon setting E_F as the reference for energy, the CB-offset eventually turns out to be $\Delta E_C = \Delta E_g/2$, where ΔE_g is the difference in the bandgaps of AlGaN and GaN. Realistic band-offsets could therefore be extracted using Eq. (7). Hence, simple GGA calculations are sufficient to conclude the insignificant variation of the CB-offset with the strain in GaN, as is evident from Fig. 6.

The conclusions from the above are two-fold. First, we note that the hybrid functional bandgaps may be estimated from the relaxed GGA gaps, and the straight-line parameters are extracted from Figs. 1 and 4. Second, we find that the variation of AlGaN bandgap with strain (up to 1%) turns out to be less than 2%; which is not materially significant for the purpose of device design. Moreover, the AlGaN/GaN CB offset experiences negligible variation due to strain in the GaN layer (see Fig. 6). The question now is whether this translates to a similarly small variation in final device performance. In the following section, we answer this by studying the effect of the strain on a key device metric.

3. 2DEG density calculations

The impact of GaN layer strain was seen to be negligible when it comes to band gaps and offsets. However, this strain could conceivably affect device performance through parameters other than the offset; namely, the piezoelectric polarization. The effect of the strain must finally be measured in terms of the modulation of critical device parameters. To that end, we study the impact of the GaN substrate strain on the 2DEG density at the $Al_xGa_{1-x}N$/GaN heterointerface.

Our approach involves calculation of the polarization charge in the heterostructure by including the GaN layer strain, the values of ΔE_C calculated above, and analytical evaluation of the 2DEG density N_s thence. It is well-known

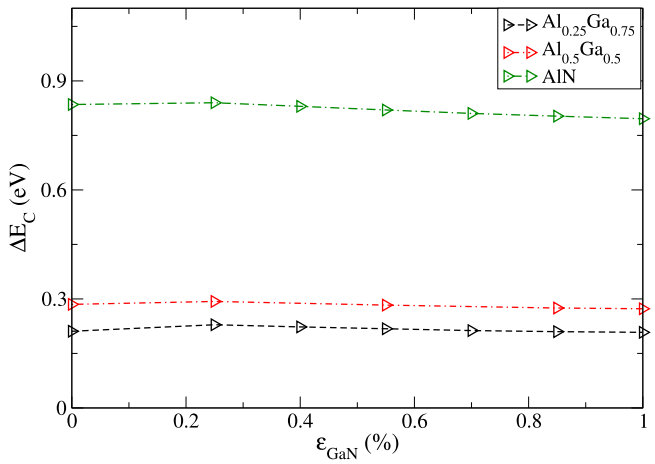

Fig. 6. (Color online) Simple GGA calculations show the weak variations in the band-offset with tensile strain in GaN.

that the total polarization charge (σ_0) at the $Al_xGa_{1-x}N$/relaxed-GaN heterointerface is given by the expression:

$$\sigma_0 = |P_{sp0}(\text{AlGaN}) - P_{sp0}(\text{GaN}) + P_{pe0}(\text{AlGaN})|. \quad (10)$$

Here, P_{sp0} (P_{pe0}) denotes the spontaneous (piezoelectric) polarization charge which is obtained from the empirical expressions.[1)]

In the next step one introduces strain in the GaN layer, and this will inflict an additional piezoelectric polarization charge P_{pe}(GaN) in the GaN layer itself. Further, it necessitates a recalculation of the piezoelectric polarization charge term in AlGaN layer P_{pe0}(AlGaN). The total polarization charge is thus modified as:

$$\sigma = |P_{sp0}(\text{AlGaN}) - P_{sp0}(\text{GaN}) + P_{pe}(\text{AlGaN}) - P_{pe}(\text{GaN})|. \quad (11)$$

The respective piezoelectric polarization charges are given by the following expressions

$$P_{pe}(\text{AlGaN}) = 2\left(\frac{a' - a(\text{AlGaN})}{a(\text{AlGaN})}\right) \times \left(e_{31}(\text{AlGaN}) - e_{33}(\text{AlGaN})\frac{C_{13}(\text{AlGaN})}{C_{33}(\text{AlGaN})}\right), \quad (12)$$

$$P_{pe}(\text{GaN}) = 2\left(\frac{a' - a(\text{GaN})}{a(\text{GaN})}\right) \times \left(e_{31}(\text{GaN}) - e_{33}(\text{GaN})\frac{C_{13}(\text{GaN})}{C_{33}(\text{GaN})}\right). \quad (13)$$

Here, a denotes the bulk lattice constant, C_{13} (C_{33}) is the elastic constant, and e_{31} (e_{33}) is the piezoelectric constant. The strained GaN lattice parameter a' is given by: $a' = a(\text{GaN}) + \varepsilon \cdot a(\text{GaN})$ with ε as the process-induced strain in the GaN layer.

Indeed, the strain in the underlying GaN layer would not influence AlGaN surface state parameters. The expression for the 2DEG density is given by:[9,11,28,29)]

$$N_s = \frac{\sigma + \frac{\epsilon(\Delta E_C - E_d)}{q d_{\text{AlGaN}}}}{1 + \frac{\epsilon}{q d_{\text{AlGaN}}} \cdot \left(\frac{1}{D} + \frac{1}{n_0}\right)}, \quad (14)$$

where D is the 2D density of states, ϵ is the GaN dielectric permittivity, and d_{AlGaN} is the barrier thickness. A constant surface donor density below the donor level E_d (eV) with the population n_0 states per unit area and energy ($\text{cm}^{-2}\,\text{eV}^{-1}$) is considered.[9)]

Figure 7 shows the variation of the calculated 2DEG density as a function of the barrier thickness (strain in the GaN substrate is a parameter). We find that the 2DEG density increases significantly (modestly) with the barrier thickness (strain in the GaN layer). How the Al mole fraction and the underlying GaN layer strain modulate the polarization charge is depicted in Fig. 8. From these two figures, one can hypothesize that the strain in the GaN layer modulates the strain in the AlGaN layer, and thence the piezoelectric polarization therein [which is also seen from Eqs. (10)–(13)]. The impact of the variation of ΔE_C with

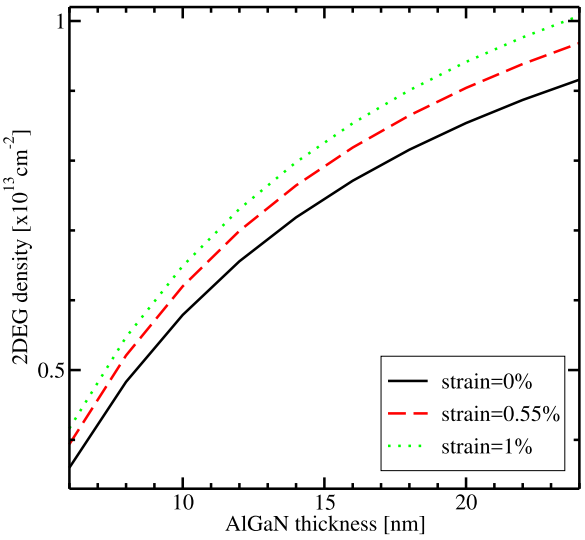

Fig. 7. (Color online) The increase of the 2DEG density value with the barrier thickness is shown. The strain in the GaN layer is used as a parameter.

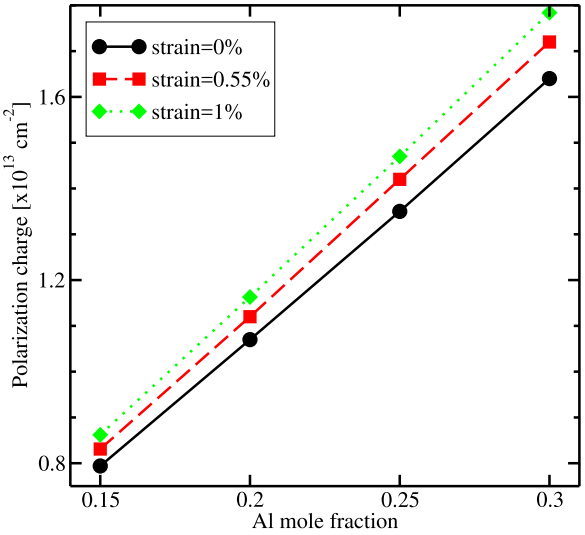

Fig. 8. (Color online) The increase of the polarization charge with the Al mole fraction is shown. The strain in the GaN layer is used as a parameter.

strain is not so significant in determining the carrier concentration. Figure 7 also shows the 1% GaN layer strain to cause almost 9% increment in the 2DEG density, when $d_{\mathrm{AlGaN}} = 24$ nm.

In Fig. 7 the barrier layer thickness is shown to be maximum 24 nm. Of course, in order to accurately calculate the polarization charge, one must additionally incorporate the AlGaN layer strain relaxation effects if both Al mole fraction and d_{AlGaN} are sufficiently high.[30] Indeed, to achieve the performance optimization of the final AlGaN/GaN based HEMTs, a thick but dislocation-free AlGaN layer will be required. In such a case, a moderate value of the Al mole fraction (like in our case, 0.25) is needed to have a highly efficient and reliable HEMT structures, thus by minimizing AlGaN layer strain relaxation. Moreover, layers of low Al fraction are also beneficial due to reduced amounts of oxygen at the AlGaN top surface. As one can ignore the impact of minor variations of ΔE_C on the carrier density, an AlGaN/GaN heterostructure having a lower value of the Al mole fraction will undergo a higher increment in the 2DEG density due to the strain effect in the underlying GaN layer. This is because when the mole fraction decreases, σ decreases significantly: both the terms P_{sp0}(AlGaN) and P_{pe}(AlGaN) will be reduced. In such a case, the part of the polarization charge which is influenced by the strain in the GaN layer becomes dominant. In this context, our calculations predict the maximal increment in the 2DEG density is as much as 17% for $x = 0.15$. The bare surface barrier height, which is simply given by the equation: $q\Phi_B = \frac{N_s}{n_0} + E_d$, will also increase due to the GaN layer strain.

4. Conclusion

The properties of $Al_xGa_{1-x}N$/GaN heterostructures have been computed for the case where the underlying GaN is tensile strained. Bandgaps are calculated using the density functional theory in the GGA regime, which is computationally inexpensive, and the hybrid functional Gau–PBE regime which is computationally heavy but matches experiment better. Simple relations connecting the bandgap trends from these two methods have been derived. These lead to a comprehensive and accurate method of predicting bandgaps of strained AlGaN using the inexpensive GGA calculations. The polarization charge, and thereby the 2DEG concentration at the AlGaN/GaN interface, are then calculated analytically. It is found that the band-offsets have a weak dependence on the GaN layer strain, because the latter induces roughly the same amounts of shift in the GaN and AlGaN CB edges. On the other hand, substantial enhancement in the 2DEG density is possible when the GaN layer is strained—this is due to the consequent increase in polarization. It is also observed that for higher values of the Al mole fraction, the polarization charge is large anyway and the relative boost due to the GaN layer strain becomes smaller. Our work suggests that strain in the GaN layer—which might be unintentional today—could be used to achieve higher 2DEG density in the future if it can be engineered controllably. Lastly, it provides a framework to extend this effect to other III-N heterstructures.

Acknowledgments

M.D. and P.G. would like to acknowledge Center for Computational Materials Science, Tohoku University, Japan and IISER Pune, India for computing facility. PG would like to acknowledge DST-Nanomission, India grant nos. SR/NM/NS-15/2011 and SR/NM/NS-1285/2014 for funding. S.M., J. G., D.S., A.L. and S.G. would like to acknowledge support from MHRD and DST through the IMPRINT program, DST through the Smart Grid Mission Innovation program, and MeitY through the Nanoelectronics Network for Research and Applications.

ORCID iDs

Mihir Date https://orcid.org/0000-0002-9778-6104
Swaroop Ganguly https://orcid.org/0000-0003-1184-8421

1) O. Ambacher et al., J. Appl. Phys. **85**, 3222 (1999).
2) J. P. Ibbetson, P. T. Fini, K. D. Ness, S. P. DenBaars, J. S. Speck, and U. K. Mishra, Appl. Phys. Lett. **77**, 250 (2000).
3) A. Dadgar, J. Blaesing, A. Diez, A. Alam, M. Heuken, and A. Krost, Jpn. J. Appl. Phys. **39**, L1183 (2000).
4) M. Azize and T. Palacios, J. Appl. Phys. **108**, 023707 (2010).

5) H.-P. Lee, J. Perozek, L. D. Rosario, and C. Bayram, Sci. Rep. **6**, 37588 (2016).
6) A. Kadir, C. C. Huang, K. E. K. Lee, E. A. Fitzgerald, and S. J. Chua, Appl. Phys. Lett. **105**, 232113 (2014).
7) H. F. Liu, S. B. Dolmanan, T. N. Bhat, and S. Tripathy, Appl. Phys. Lett. **106**, 176101 (2015).
8) L. Gordon, M.-S. Miao, S. Chowdhury, M. Higashiwaki, U. K. Mishra, and C. G. Van de Walle, J. Phys. D: Appl. Phys. **43**, 505501 (2010).
9) N. Goyal, B. Iniguez, and T. A. Fjeldly, Appl. Phys. Lett. **101**, 103505 (2012).
10) N. Goyal and T. A. Fjeldly, J. Appl. Phys. **113**, 014505 (2013).
11) J. Ghosh, A. Laha, D. Saha, and S. Ganguly, Proc. EUROSOI-ULIS, 2017 , p. 156.
12) J. Ghosh, D. Saha, S. Ganguly, and A. Laha, Int. J. RF Microwave Comput.-Aided Eng. **28**, e21455 (2018).
13) P. Giannozzi et al., J. Phys.: Condens. Matter **21**, 395502 (2009).
14) P. Giannozzi et al., J. Phys.: Condens. Matter **29**, 465901 (2017).
15) J. P. Perdew, K. Burke, and M. Ernzerhof, Phys. Rev. Lett. **77**, 3865 (1996).
16) H. J. Monkhorst and J. D. Pack, Phys. Rev. B **13**, 5188 (1976).
17) H. Angerer et al., Appl. Phys. Lett. **71**, 1504 (1997).
18) W. Shan, J. W. Ager, K. M. Yu, W. Walukiewicz, E. E. Haller, M. C. Martin, W. R. McKinney, and W. Yang, J. Appl. Phys. **85**, 8505 (1999).
19) D. Brunner, H. Angerer, E. Bustarret, F. Freudenberg, R. Höpler, R. Dimitrov, O. Ambacher, and M. Stutzmann, J. Appl. Phys. **82**, 5090 (1997).
20) N. Nepal, J. Li, M. L. Nakarmi, J. Y. Lin, and H. X. Jiang, Appl. Phys. Lett. **87**, 242104 (2005).
21) R. Gonzàlez-Hernàndez, A. Gonzàlez-Garcìa, D. Barragàn-Yani, and W. Lòpez-Pèrez, Appl. Surf. Sci. **314**, 794 (2014).
22) Z. Dridi, B. Bouhafs, and P. Ruterana, Semicond. Sci. Technol. **18**, 850 (2003).
23) P. G. Moses, M. Miao, Q. Yan, and C. G. Van de Walle, J. Chem. Phys. **134**, 084703 (2011).
24) K. Shim, D. N. Talwar, and H. J. Moh, Solid State Commun. **97**, 315 (1996).
25) F. Yun, M. A. Reshchikov, L. He, T. King, H. Morkoc, S. W. Novak, and L. Wei, J. Appl. Phys. **92**, 4837 (2002).
26) A. Kyrtsos, M. Matsubara, and E. Bellotti, Phys. Rev. B **99**, 035201 (2019).
27) M. Gao, S. T. Bradely, Y. Cao, D. Jena, Y. Lin, S. A. Ringel, J. Hwang, W. J. Schaff, and L. J. Brillson, J. Appl. Phys. **100**, 103512 (2006).
28) J. Ghosh and S. Ganguly, Jpn. J. Appl. Phys. **57**, 080305 (2018).
29) J. Ghosh, J. Phys. Commun. **2**, 125010 (2018).
30) N. Goyal and T. A. Fjeldly, J. Appl. Phys. **113**, 014505 (2013).